08,05

Investigation of structural and hysteresis properties of oxidized permalloy films

© I.V. Blinov, Yu.V. Korkh, T.V. Kuznetstova, D.I. Devyaterikov, I.K. Maksimova, R.M. Falahutdinov, A.Yu. Istomina

M.N. Mikheev Institute of Metal Physics, Ural Branch, Russian Academy of Sciences, Yekaterinburg, Russia

E-mail: blinoviv@mail.ru

Received February 27, 2025
Revised March 5, 2025
Accepted March 6, 2025

The paper presents the results of the study of structural and hysteresis properties of permalloy films. The kinetics of oxide formation on the film surface under different oxidation conditions has been studied. New experimental data on the structure and magnetic properties of the synthesized compounds have been obtained. In permalloy films oxidized in air, it was found that as the temperature of thermomagnetic treatment increases, $NiFe_2O_4$ oxides and amorphous iron oxyhydroxide groups are mainly formed in the samples. As the annealing temperature is further increased, the oxides formed on the surface of permalloy films are iron oxides (predominantly α-Fe_2O_3). The regularities of hysteresis properties change at varying annealing temperature have been determined. The conditions of formation of the exchange shift of the hysteresis loop in oxidized permalloy films have been established.

Keywords: permalloy, unidirectional anisotropy, oxides, thermomagnetic treatment.

DOI: 10.61011/PSS.2025.03.60884.41-25

1. Introduction

Modern magnetic nanomaterials consisting of ultrathin ferromagnetic (FM) and antiferromagnetic (AF) or ferrimagnetic (FI) layers are of great interest to researchers. Thus, for example, in a FM layer bound with an AF layer in such laminar structures, unidirectional magnetic anisotropy occurs due to exchange interaction at the FM/AF interface. Magnetic hysteresis loop of such structure has a higher coercive force (H_c) and appears to be shifted along the magnetic field axis at the exchange bias field value (H_{ex}). The unidirectional anisotropy effect is the basis for practical applications primarily in storage systems such as magneto-resistive random access memory and spin valves. The exchange bias effect in these systems has a crucial significance because it ensures a stable homogeneous magnetized state [1–4]. However, for successful practical application of laminar structures with exchange bias, it is required to study the dependence of structural and magnetic properties of the structures on the type and efficiency of interlayer bonding that in turn is defined by the structural and chemical state of layers and interlayer boundaries.

In particular, for $Ni_{80}Fe_{20}$ permalloy films that serve as the basis for preparing various functional magnetoresistive media [1,5], it has been shown previously that, depending on the preparation, oxidation and annealing conditions, AF and FI iron oxides with various valence (Fe_2O_3, Fe_3O_4) are formed in permalloy films, AF and FI nickel oxides (NiO, $NiFe_2O_4$) might be also formed, moreover, Ni hydroxides are formed additionally during oxidation in air [6–10]. Thus, the exchange bias effect may be implemented in permalloy-oxide systems. Magnetic annealing is one of the known methods for forming AF/FM exchange coupling in lamellar film systems.

This study investigates structural and magnetic properties in oxidized permalloy films in various thermomagnetic treatment conditions.

2. Experiment

Nanostructured $Ni_{80}Fe_{20}$ films were prepared by magnetron sputtering using the MPS-4000-C6 Ulvac sputtering system on the $(10\bar{1}2)$ Al_2O_3 single-crystal sapphire substrates. Ta, 5 nm in thickness, was used as a buffer and protective layer.

The following samples were prepared:

1. Al_2O_3/Ta(5)/$Ni_{80}Fe_{20}$(20)/Ta(5);

2. Al_2O_3/Ta(5)/$Ni_{80}Fe_{20}$(20) then holding in a magnetron chamber at an oxygen pressure of 10 Pa for 30 min. Then — Ta(5) layer sputtering for protection against oxidation.

3. Al_2O_3/Ta(5)/$Ni_{80}Fe_{20}$(20) — these samples are not covered with a protective Ta layer.

Numbers in brackets hereinafter denote layer thicknesses in nm.

Structural investigations were performed using the PANalytical Empyrean X-ray diffractometer in CoK_α radiation.

The Solver Next scanning probe microscope was used to determine surface topography and magnetic microstructure, the recorded surface profile images were processed in Image Analysis. Investigations were performed at room temperature and humidity of 25−30%, silicon probes with CoCr magnetic coating, standard tip curvature radius less

than 30 nm and cantilever resonance frequency 75 kHz were used. Magnetic-force images were obtained in non-contact mode using a double-pass technique to visualize nonuniformity of magnetic forces acting on the probe from the sample surface without artefacts induced by the sample topography. During the second pass, the cantilever was lifted at each scan point at the distance $d_z = 200$ nm from the sample surface. Long-range magnetic forces contribute to variation of the cantilever vibration phase in the second pass and form the distribution of the z-component of the magnetic force gradient over the sample surface.

Oxide formation kinetics in the samples was studied using the Raman-scattering spectroscopy. Raman scattering (RS) spectra were measured using the Confotec MR200 (SOL Instruments) confocal Raman microscope with 532 nm laser excitation. Laser power on the sample surface was 76 mW. Integration time was 30–40 s, number of averages was 5. A 40× (Olympus) lens with numerical aperture 0.75 was used. Confocal opening diameter was 100 mm. A 1200/600 line diffraction grating and electrically cooled charged-coupled device detector were used for spectra recording.

Thermomagnetic treatment of group 2 samples was performed on an original design system at 10–4 Pa in 2 kOe constant magnetic field applied in the sample plane in the temperature range of 150–550 °C during 30 min. The same system was used for oxidation of group 3 samples in the temperature range of 150–300 °C at atmospheric pressure. Thermomagnetic treatment time was 1 h.

Hysteresis properties of films were studied using the ABM-1 computer-assisted vibration magnetometer in the auto mode at room temperature. Coercive force H_c and bias field H_{ex} were defined from hysteresis loops as the loop half-width and hysteresis loop center shift with respect to zero along the magnetic field axis. Direction of the magnetic field for measurement coincided with that of the magnetic field applied during thermomagnetic treatment.

3. Findings and discussion

Figure 1 shows an X-ray diffraction pattern of Al_2O_3/Ta(5)/$Ni_{80}Fe_{20}$(20)/Ta(5) sample 1. Besides reflections from the Al_2O_3 substrate, there is only one intense reflection (111) from the $Ni_{80}Fe_{20}$ FCC lattice indicating a crystal texture of the ⟨111⟩ type permalloy layer. $Ni_{80}Fe_{20}$ FCC lattice parameter $a = 0.355$ nm corresponds to that of permalloy [11]. Crystallite size determined using the Scherrer equation [12] is approximately 20 nm.

Degree of perfection of the ⟨111⟩ texture was evaluated using the rocking curve method. Figure 1 shows a rocking curve measured with 2θ fixed at the value corresponding to the reflection of (111) $Ni_{80}Fe_{20}$ and with variation of the initial beam incidence angle ω. Form of the rocking curve corresponds to the ⟨111⟩ axial texture. γ determined from the rocking curve as full width at half maximum and characterizing the texture perfection or disorientation angle

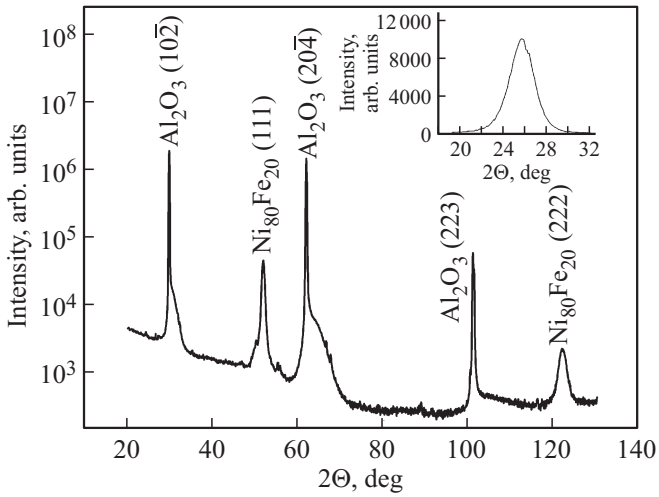

Figure 1. X-ray diffraction pattern of the Al_2O_3/Ta(5)/$Ni_{80}Fe_{20}$(20)/Ta(5) sample The inset shows a rocking curve measured on the (111) diffraction line of$Ni_{80}Fe_{20}$.

of the [111] crystallite axes from the texture axis is equal to 2.9°, which corresponds to the ⟨111⟩ high-perfection structure formed in the test samples.

It is known that surface condition of nanocrystalline films affects considerably their hysteresis properties [13]. Texture nonuniformity in lamellar polycrystalline films may be due to the size of individual crystallites and to the surface condition of a substrate or underlying layers. Small thickness of the protective Ta layer suggests that the layer follows the texture of the underlying permalloy layer and, thus, indirect information concerning the microstructure may be obtained in films using AFM. Numerical description of surface texture, rms surface roughness R_q, was used as a criterion for surface condition assessment.

Figure 2 shows an image of the surface of sample 1 and an example of surface treatment to determine the mean crystallite size. The samples have a low rms surface roughness $R_q = 0.25$ nm, mean gran size is 20.8 nm, which agrees with the X-ray measurement data.

Examination of the magnetic properties of sample 1 showed that saturation magnetization M_s was 86 emu/g and coercive force was $H_c = 1.5$ Oe. The obtained values are typical for permalloy films formed by magnetron sputtering [14].

An oxide layer on the permalloy surface was formed using a technique that was applied successfully by its authors to the Fe/FeO system [15]. The technique is defined as formation of an oxidized layer on the film surface by holding in a magnetron sputtering chamber in gas mixture in pre-defined conditions. The authors showed that a FeO with a thickness of about 2 nm was formed on the surface of Fe film. The study used a similar technique for oxidation of multilayer $Ni_{95}Fe_5$/NiFeO films [6]. In group 2 structures, after deposition of the tantalum and permalloy layers, working gas — oxygen — was injected

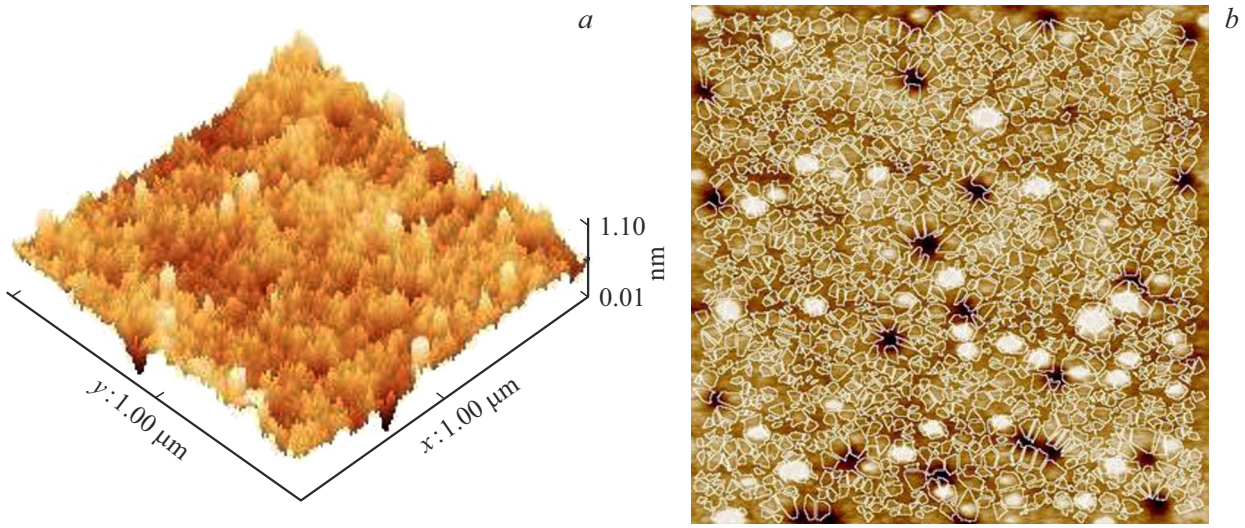

Figure 2. AFM-image of the surface of Al_2O_3/Ta(5)/$Ni_{80}Fe_{20}$(20)/Ta(5) sample: (*a*) — initial condition; (*b*) — processing in Image Analysis. Scan area size is $1 \times 1\,\mu$m.

into the magnetron sputtering chamber and, after holding and evacuation, a Ta layer was sputtered to protect the laminar structure against oxidation.

Investigation of the magnetic properties of group 2 samples showed that the saturation magnetization ($M_s = 79$ emu/g) decreased insignificantly compared with M_s of sample 1, and the coercive force remained unchanged $H_c = 1.5$ Oe. The obtained data might be indirectly indicative of a decrease in the volumetric fraction of permalloy in the oxidized samples due to surface oxidation, and the oxide layer thickness is probably 2 nm maximum [6,8]. Film surface topography investigations (mean grain size 20.4 nm, $R_q = 0.23$ nm) gave similar data compared with group 1 samples. The X-ray diffraction pattern has no any additional reflections, besides the (111) reflection from the $Ni_{80}Fe_{20}$ FCC lattice, which is probably due to the X-ray amorphous state of the formed oxides.

Oxide formation was verified using the Raman-scattering spectroscopy. Since a focused laser beam in the Raman-scattering spectroscopy method can penetrate partly under the detection surface through a thin protective Ta layer, then it was possible to get information concerning the presence of $Ni_{80}Fe_{20}$ film oxide vibrations. Raman scattering peaks corresponding to vibrations of the following fundamental phases were detected on the surface of test samples: α-Fe_2O_3, Fe_3O_4, $NiFe_2O_4$. Figure 3 shows the Raman scattering spectra of sample groups 1, 2, 3 after sputtering.

For the Al_2O_3/Ta(5)/$Ni_{80}Fe_{20}$(20)/Ta(5) samples of group 1 (spectrum *a* in Figure 3), no pronounced Raman peaks were detected, which indicates that there are no oxide phases on the permalloy film surface. On the other hand, Raman peaks occur on the surface of group 2 sample (spectrum *b* in Figure 3) with the most intense of them being vibration peaks at 557 cm^{-1} and 678 cm^{-1} that correspond to the $NiFe_2O_4$ phase [16,17] and confirm oxidation of the permalloy surface. Vibration peaks of the α-Fe_2O_3, Fe_3O_4phases were also detected and were induced by the interaction between Fe atoms (one of the $Ni_{80}Fe_{20}$ film components) and oxygen and by formation of Fe oxides with different valence [18]. No FeOOH phase vibrations were detected. Thus, it is fair to say that α-Fe_2O_3, Fe_3O_4, $NiFe_2O_4$, with prevailing $NiFe_2O_4$, are formed on the surface of $Ni_{80}Fe_{20}$ layer during oxidation in the magnetron chamber in extra-pure oxygen atmosphere. Since the type of magnetic ordering of the formed oxides differs from FM (α-Fe_2O_3 is antiferromagnetic and Fe_3O_4, $NiFe_2O_4$ are ferrimagnetics), then formation of unidirectional anisotropy might be expected in group 2 samples during magnetic field annealing. For this, thermomagnetic treatment of structures was performed in the temperature range from 100 °C to 550 °C for 30 min.

Magnetic hysteresis loops were obtained and temperature dependences of hysteresis properties were determined. It appeared that, as annealing temperature increases, the coercive force varies insignificantly and there is no magnetic hysteresis loop shift indicative of the presence of exchange coupling at the interface. The presence of exchange coupling with AF would induce a shifted hysteresis loop and/or increase in the coercive force of the ferromagnetic layer. A small growth of H_c to 10 Oe at the annealing temperature of 550 °C is probably caused by changes of film microstructure [19,20]. As the annealing temperature increases, $\Delta M_s/M_s^0$ ($\Delta M_s = M_s - M_s^0$, M_s is the saturation magnetization of the sample after thermomagnetic treatment, M_s^0 is the saturation magnetization of the initial sample) remains the same showing that the volumetric fraction of permalloy remains unchanged, thus, mutual diffusion at the permalloy-oxide interface is excluded. The absence of hysteresis loop may be due to a low thickness of the oxide layer. According to the Michaeljohn and Bean

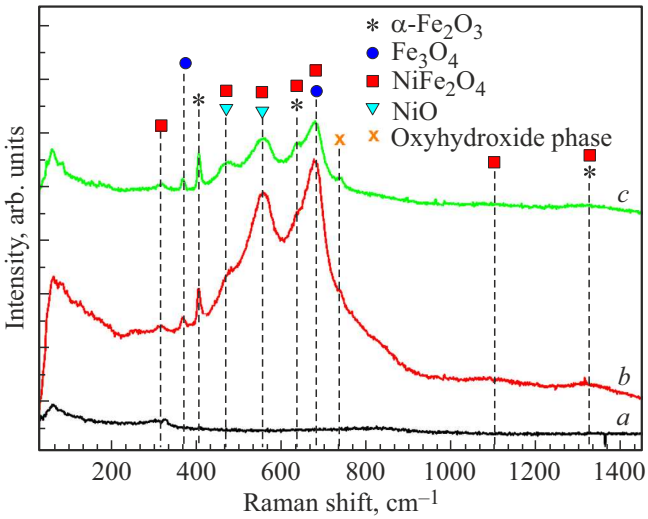

Figure 3. Raman scattering spectra of the Al_2O_3/Ta(5)/$Ni_{80}Fe_{20}$(20) samples: *a*) group 1, *b*) group 2, *c*) group 3.

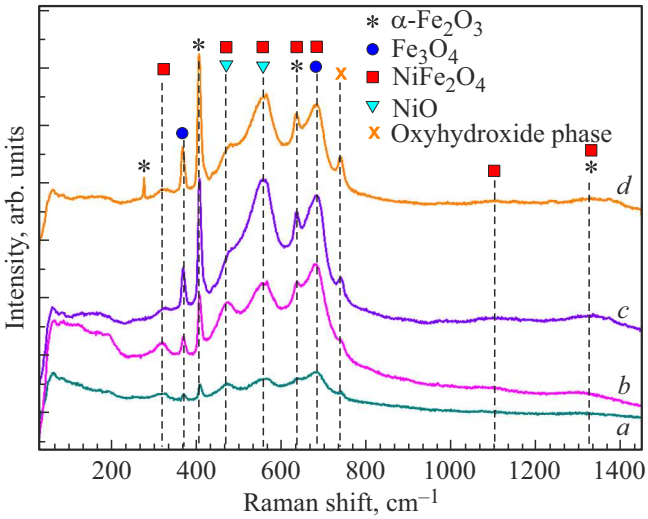

Figure 4. Raman scattering spectra of the Al_2O_3/Ta(5)/$Ni_{80}Fe_{20}$(20) films after heat treatment: *a*) 200 °C, *b*) 250 °C, *c*) 280 °C, *d*) 300 °C — 60 min.

model [5], the exchange shift of hysteresis loop occurs when $K_{AF} \cdot t_{AF} \rangle J_{ex}$ is satisfied, where K_{AF} is the AF anisotropy constant, t_{AF} is the AF thickness, J_{ex} is the exchange interaction energy surface density. It this condition is not met, then there will be no loop shift, but the coercive force will grow. However, H_c doesn't increase either. This effect is probably due to a disordered magnetic state of the formed oxides and, therefore, they don't contribute to the growth of H_c.

Behavior of structural and magnetic properties varies considerably in the Al_2O_3/Ta(5)/$Ni_{80}Fe_{20}$(20) samples from group 3 during permalloy surface oxidation in air followed by heat treatment. RS spectrum of sample 3 is qualitatively similar to that of group 2 sample (Figure 3, spectra *b* and *c*), however, vibration peaks at 558 cm^{-1} and 680 cm^{-1} of the $NiFe_2O_4$ phase are less intense and wider compared with the peaks of $NiFe_2O_4$ in sample 2, which is indicative of a low concentration of $NiFe_2O_4$ on the permalloy film surface during natural oxidation in air. Vibration peaks of the α-Fe_2O_3, Fe_3O_4 phases were detected due to the interaction between Fe atoms of the permalloy film and air. Moreover, additional peak occurs at 739 cm^{-1} due to vibrations of amorphous oxyhydroxide groups of iron [21].

Figure 4 shows Raman spectra of sample 3 after annealing at 200 °C, 250 °C, 280 °C, 300 °C — 60 min. Thus, after annealing at (T_a) = 200 °C, RS spectrum (Figure 4, spectrum *a*) is similar to that of the film after sputtering (Figure 3, spectrum *c*): a peak at 680 cm^{-1} of the $NiFe_2O_4$ phase is the most intense, there is also an oxyhydroxide peak. However, peak intensity caused by the $NiFe_2O_4$ phase vibration at 324 cm^{-1} becomes higher, which clearly indicates the growth of concentration of this oxide during annealing.

With further increase in T_a, the view of Raman spectra varies considerably. There are changes in peak positions and height, which unambiguously indicates that film structure and composition are different as heat treatment temperature increases (spectra *b, c, d* in Figure 4). Thus, at T_a = 250 °C, a peak at 680 cm^{-1} corresponding to the $NiFe_2O_4$ phase is also the most intense one, but intensities of Fe_3O_4 and α-Fe_2O_3 (370 cm^{-1} and 408 cm^{-1}) peaks increase considerably at the same time, which is indicative of the growth of concentration of iron oxides with different valence. Oxyhydroxide peak at 740 cm^{-1} is faint. Raman spectrum of the film after heat treatment at T_a = 280 °C has a quick growth of intensity of the Fe_3O_4 and α-Fe_2O_3 peaks at 370 cm^{-1} and 408 cm^{-1} and also increasing intensity of oxyhydroxide phase vibrations at 740 cm^{-1}, which is indicative of the growth of iron oxide phases as the annealing temperature increases. Vibration peaks of α-Fe_2O_3 (407 cm^{-1}) and of group NiO [22,23] in the $NiFe_2O_4$ phase (559 cm^{-1}) are most intense, which indicates that iron and nickel oxides (individual components of the $Ni_{80}Fe_{20}$ film) are formed. For the film annealed at T_a = 300 °C, a peak of α-Fe_2O_3 at 407 cm^{-1} is most intense, and an additional peak of α-Fe_2O_3 also occurs at 277 cm^{-1}. A peak of oxyhydride group vibrations grows and narrows considerably at 740 cm^{-1}. Peaks at 553 cm^{-1} and 682 cm^{-1} corresponding to $NiFe_2O_4$ at T_a = 300 °C broaden compared with the sample at T_a = 280 °C, which suggests a lower degree of crystallinity and deformation of the $NiFe_2O_4$ phase as the annealing temperature grows. Splitting of the peak at 553 cm^{-1} is an interesting finding that is associated with distortion of vibrations at various lengths of atomic bonds Fe-O and Ni-O within the $NiFe_2O_4$ structure [24]. Intensity growth and narrowing of peaks corresponding to the α-Fe_2O_3 phase at T_a = 300 °C are indicative of the growth of concentration of this phase on the sample surface. Thus, according to the Raman-scattering spectroscopy data, it was found that, as the annealing temperature grew to 250 °C, $NiFe_2O_4$ were

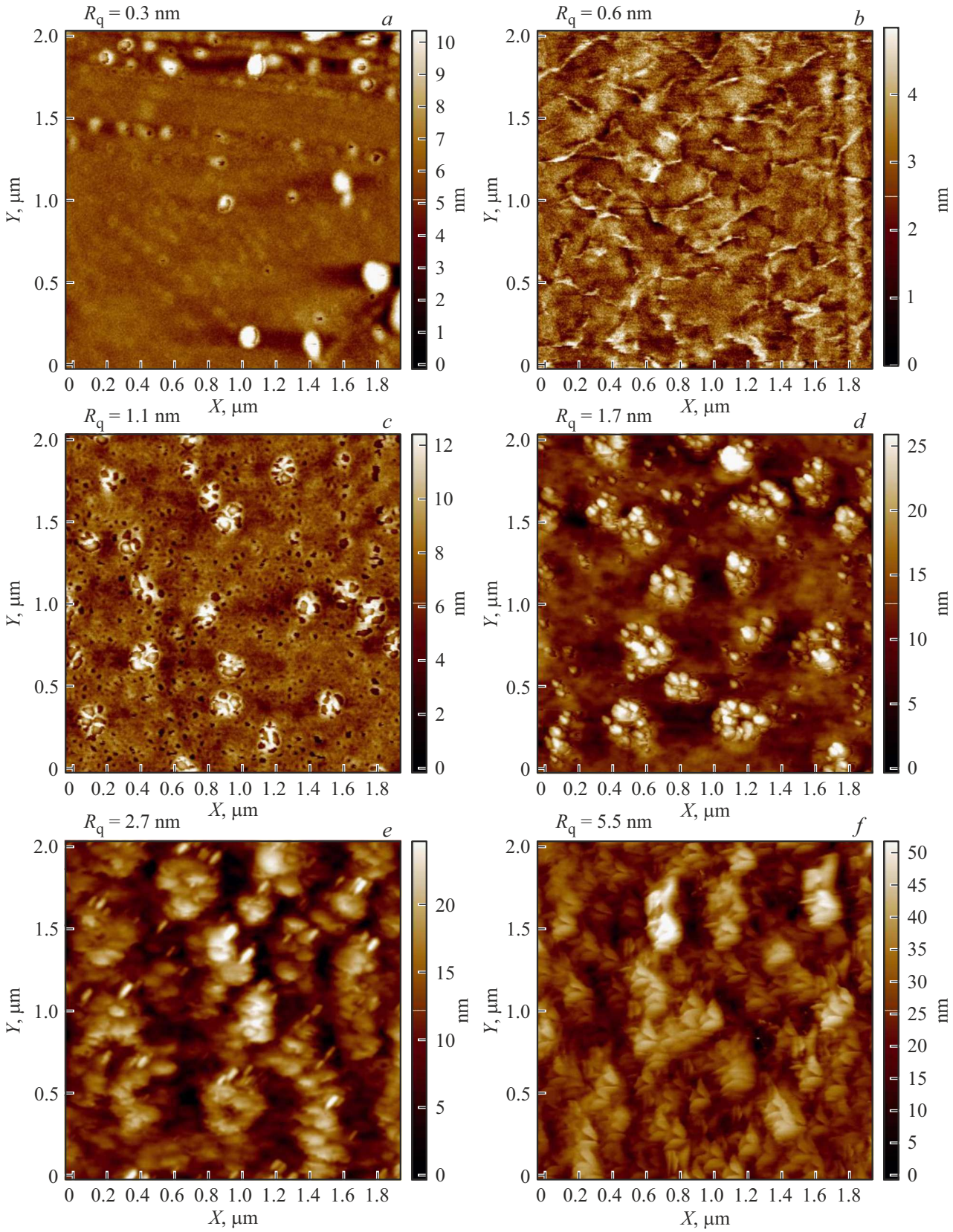

Figure 5. ACM images of Al_2O_3/Ta(5)/$Ni_{80}Fe_{20}$(20) films surface before (*a*) and after heat treatment at *b*) 150 °C, *c*) 200 °C, *d*) 250 °C, *e*) 280 °C, *f*) 300 °C — 60 min.

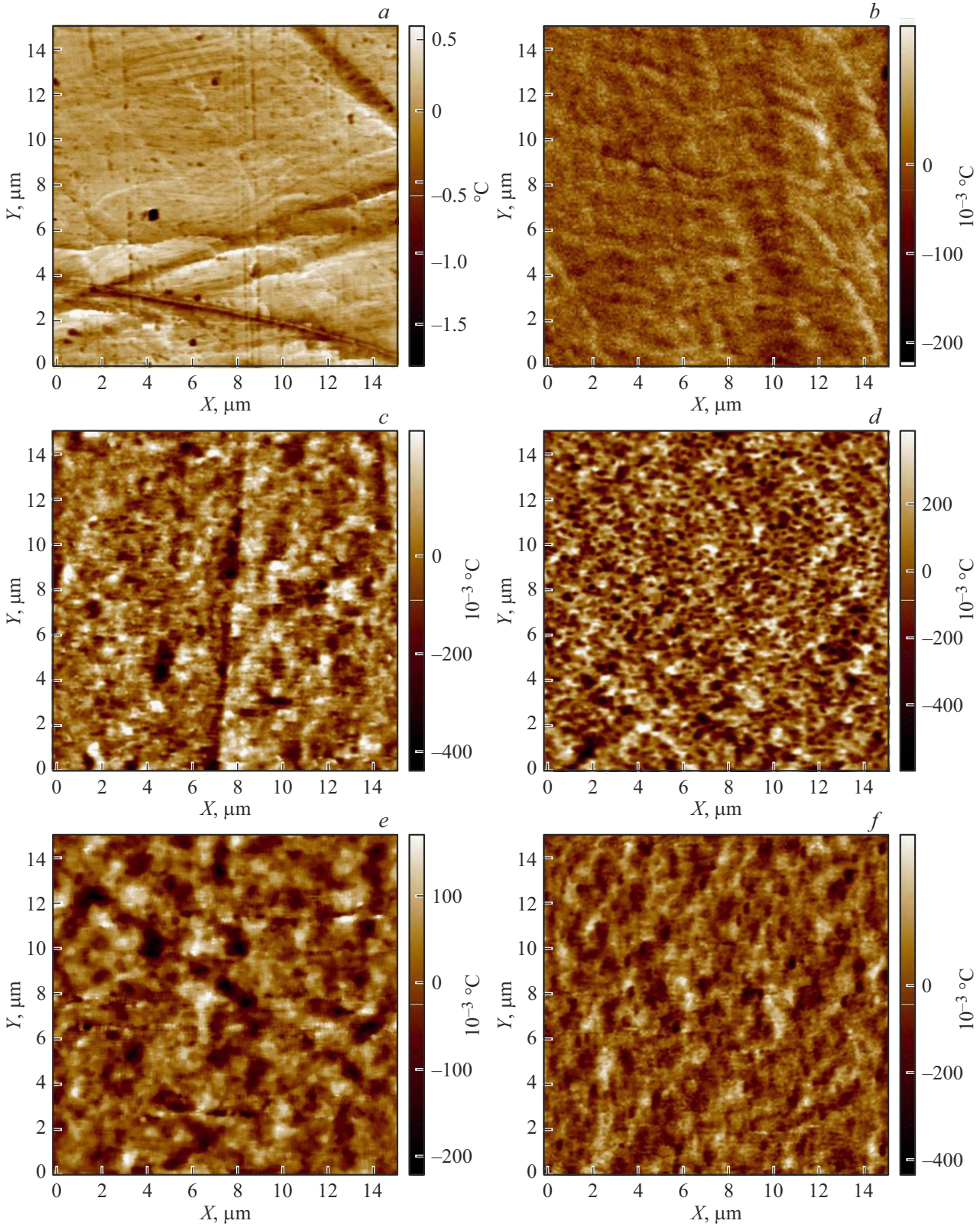

Figure 6. MFM images of Al_2O_3/Ta(5)/$Ni_{80}Fe_{20}$(20) films surface initial state (*a*) and after heat treatment at *b*) 150 °C, *c*) 200 °C 2, *d*) 250 °C, *e*) 280 °C, *f*) 300 °C — 60 min.

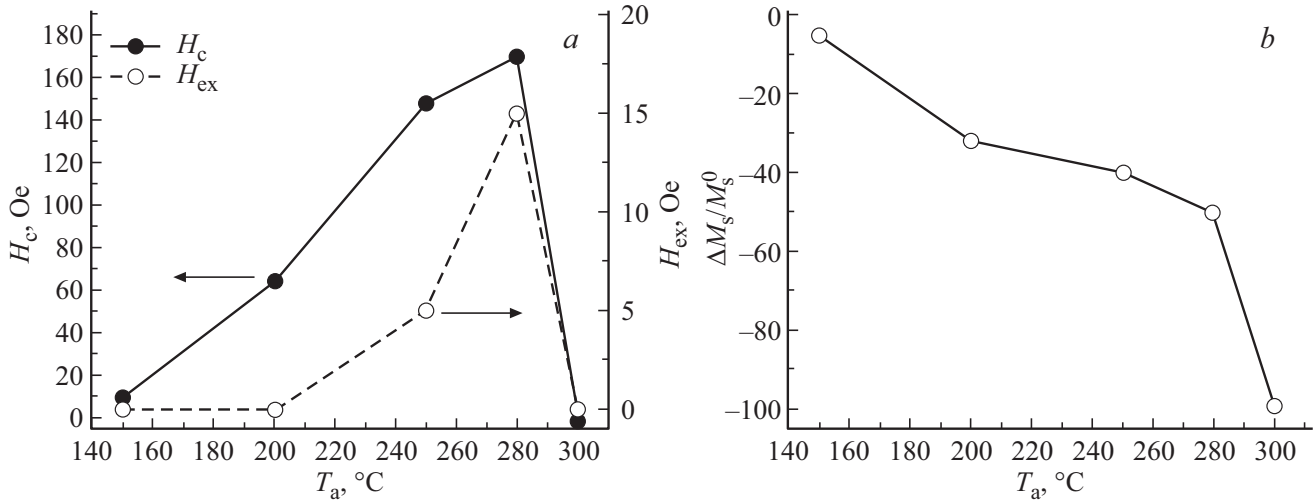

Figure 7. Temperature dependences H_c and H_{ex} (a) and DMs/Ms0 (b) of the Al_2O_3/Ta(5)/$Ni_{80}Fe_{20}$(20) samples.

primarily formed in the samples. With further increase in the annealing temperature to 300 °C, oxides being formed on the $Ni_{80}Fe_{20}$ film surface are iron oxides (primarily α-Fe_2O_3). Prevailing formation of Fe_2O_3 compared with $NiFe_2O_4$ and NiO may be due to a higher enthalpy of formation of Fe_2O_3 (1.84 eV/atom) compared with $NiFe_2O_4$ (1.37 eV/atom) and NiO (1.01 eV/atom).

Figure 5 shows AFM images of the surface and values of R_q for group 3 samples before and after thermomagnetic treatment $T_a = 150$, 200, 250, 280, 300 °C — 60 min.

As the heat treatment temperature increases, the surface structure undergoes considerable changes: film surface becomes rough, clusters, that are presumably oxide phases, are formed and become larger. For the sample annealed at $T_a = 200$ °C, the size of such clusters is maximum 100–200 nm, while the sample at $T_a = 280$ °C is characterized by higher columnar clusters with the base of about 400 nm and cylindrical needle-shape buildup on top. As the annealing temperature grows to 300 °C, the surface texture consists of evenly arranged „flower-like“ phases oriented along the magnetic field applied during annealing. The sample surface is structured and is characterized by the largest $R_q = 5.5$ nm. According to [25–27], such ordered and oriented „flower-like“ phases are α-Fe_2O_3. Thus, the atomic-force microscopy results support the Raman-scattering spectroscopy data in that α-Fe_2O_3 clusters are mainly formed in the samples as the annealing temperature increases.

Magnetic force microscopy (MFM) displays film microstructure. Figure 6 shows magnetic-force images of films before and after thermomagnetic treatment. Contrast in the MFM images is caused by local magnetization distribution in the sample. Lighter areas correspond to regions with higher magnetization.

Before annealing, the samples have an inhomogeneous magnetic structure in the form of low-contrast bands (Figure 6, a) typical of this material [28,29]. The bands are about 0.7–0.8 μm in width. After $T_a = 150$ °C (Figure 6, b), the banded magnetic structure is maintained, but magnetic inhomogeneities become less contrast in the MFM image. With further increase in T_a (Figure 6, *c, d, e, f*), the magnetic-force images take a form known as the „magnetic ripple“ [29]. Such type of magnetic structure in the magnetic-force images is caused by the competition of irregular magnetic anisotropies that facilitate the inhomogeneous magnetization [30,31]. The film annealed at $T_a = 200$ °C is characterized by a larger magnetic „ripple“, and for the sample after $T_a = 250$ °C, smaller dark areas contrasting with the surface appear, which indicates that a magnetic phase with lower magnetization is formed. Dark areas in the MFM images correspond to oxide phases. Further increase in T_a to 280 °C leads to larger changes of the MFM contrast due to the increase in the fraction of oxide phases on the sample surface. Finally, the sample after $T_a = 300$ °C is characterized by a least contrast, smeared magnetic microstructure due to the presence of ordered oxide clusters and oxyhydroxide groups on the film surface.

The obtained data concerning structural transformations resulting from annealing are followed by corresponding modifications of the hysteresis properties of samples.

Figure 7, a shows the dependences of coercive force and bias field on thermomagnetic treatment temperature. As the annealing temperature increases, H_c grows, and the quick growth of H_c occurs at $T_a = 200$ °C ($H_c = 70$ Oe) reaching the maximum value of 175 Oe at $T_a = 280$ °C. Note that growth of H_c is followed by the decrease in $\Delta M_s/M_s^0$ that characterizes the mutual diffusion and variation of the volumetric fraction of permalloy after annealing. The corresponding temperature dependence $\Delta M_s/M_s^0$ is shown in Figure 7, b. At $T_a = 280$ °C, the initial magnetization decreases by 50 %. Such changes of magnetic properties might be attributable both to the interlayer diffusion effect and decrease in the volumetric fraction of permalloy, which is clearly indicated by the decrease in $\Delta M_s/M_s^0$, and to

formation of new magnetic phases leading to inhomogeneity of magnetic properties and growth of H_c. Formation of new oxide phases is confirmed by the Raman-scattering spectroscopy, AFM and MFM data, therefore it is suggested that growth of H_c is mainly caused by formation of magnetic-ordered α-Fe_2O_3phase with the Néel temperature ($T_N = 675\,^\circ C$) [5]. The latter is supported by the fact that starting from $T_a = 250\,^\circ C$ magnetic hysteresis loop shift occurs, though small with respect to the hysteresis loop width, it is reliably detectable. Thus, $H_{ex} = 5\,Oe$ at $T_a = 250\,^\circ C$ and $H_{ex} = 15\,Oe$ at $T_a = 280\,^\circ C$. According to the model in [32] that takes into account the grain size distribution in AF, large grains contribute to the hysteresis loop shift and smaller grains contribute to the growth of H_c. Appearance of the exchange bias at $T_a \geq 250\,^\circ C$ is probably caused by the growth of energy of antiferromagnetic α-Fe_2O_3 grains due to the increase in their size. It was found that as the annealing temperature increases, not only increase in the concentration of AF oxide, but also considerable growth of oxide crystallites take place. At $T_a = 300\,^\circ C$, oxygen concentration in the film is maximum, which is indicated by the decrease in $\Delta M_s/M_s^0$ by 100 %. It is fair to say that the film contains only Ni and Fe oxides in such annealing conditions.

4. Conclusion

X-ray diffraction, Raman-scattering spectroscopy, AFM and MFM methods were used to study the structural properties of permalloy films formed by magnetron sputtering on the Al_2O_3 single-crystal substrates. It was found that α-Fe_2O_3, Fe_3O_4, $NiFe_2O_4$, with prevailing $NiFe_2O_4$, are formed on the surface of $Ni_{80}Fe_{20}$ during oxidation in the magnetron chamber in extra-pure oxygen atmosphere. In permalloy films oxidized in air, it was found that mainly $NiFe_2O_4$ and amorphous oxyhydroxide groups of iron are formed as the thermomagnetic treatment temperature grows. With further increase in the annealing temperature, oxides being formed on the $Ni_{80}Fe_{20}$ film surface are iron oxides (primarily α-Fe_2O_3). Physical causes and patterns of modification of hysteresis properties of films with varying annealing temperature were determined. In particular, a possibility of exchange bias of a hysteresis loop in oxidized permalloy films is shown. Appearance of the exchange bias is probably caused by the growth of antiferromagnetic grain energy due to an increase in the grain size.

Acknowledgments

X-ray, AFM and MFM examinations were performed at Shared Research Facility „Test Center for Nanotechnology and Advanced Materials“ Institute of Physics of Metals, Ural Branch, Russian Academy of Sciences.

Funding

The study was supported by grant of the Russian Science Foundation, project No. 24-22-20083, and of the government of the Sverdlovsk Region.

Conflict of interest

The authors declare no conflict of interest.

References

[1] C. Zheng, K. Zhu, S.C. De Freitas. IEEE Transactions on Magnetics., **55**, 1 (2010). DOI: 10.1109/TMAG.2019.2896036
[2] L. Jogschies, D. Klaas, R. Kruppe. Sensors, **15**, *11*, 28665 (2015). (in Russian). DOI: 10.3390/s151128665
[3] T. Blachowicz, A. Ehrmann. Coatings, **11**, 1 (2021). DOI: 10.3390/coatings11020122
[4] F. Radu, H. Zabel. Exchange bias effect of ferro-/antiferromagnetic heterostructures, Magnetic Heterostructures, Berlin: Springer-Verlag, **3**, 97 (2008)
[5] R. Coehoorn. Novel Magnetoelectronic Materials and Devices: Handbook of Magnetic Materials. Amsterdam: Elsevier, **1** (2003).
[6] D.I. Anyfantis, C. Ballani, N. Kanistras, A. Barnasas, V. Kapaklis, G. Schmidt, E.T. Papaioannou, P. Poulopoulos. Coatings, **12**, 627 (2022). DOI: 10.3390/coatings12050627
[7] W. Brückner, S. Baunack, M. Hecker, J. Thomas, S. Groudeva-Zotova, C.M. Schneider. Materials Science and Engineering B, **86**, *3*, 272 (2001). DOI: 10.1016/S0921-5107(01)00696-1
[8] Z. He, Z. Li, X. Jiang, C. Wu, Y. Liu, X. Song, Z. Yu, Y. Wang, Z. Lan, K. Sun. Metals, **11**, 2061 (2021). DOI: 10.3390/met11122061
[9] M. Kitada. J. Mater Sci, **26**, 4150 (1991). DOI: 10.1007/BF02402960
[10] V.A. Vas'ko, M.T. Kief. J. Appl. Phys., **97**, 10J116 (2005). DOI: 10.1063/1.1854279
[11] V.O. Vas'kovskiy, O.A. Adanakova, A.N. Gorkovenko. Phys. Metals Metallogr., **116**, 1175 (2015). DOI: 10.1134/S0031918X15120133
[12] B.D. Cullity. Elements of X-Ray Diffraction. Addison-314 Wesley, Inc., London. (1978)
[13] Ahmad Al-Qawasmeh, Mohammad H.A. Badarneh, Abdalla Obeidat, Sufian Abedrabbo. J. Magn. Magn. Mater., **562**, 169734 (2022). DOI: 10.1016/j.jmmm.2022.169734.
[14] S. Ingvarsson, Gang Xiao, S.S.P. Parkin, W.J. Gallagher. J. Magn. Magn. Mater., **251**, *2*, 202 (2002). DOI: 10.1016/S0304-8853(02)00577-2.
[15] Jiajun Guo, Xiaonan Zhao, Zhijian Lu, Peng Shi, Yufeng Tian, Yanxue Chen, Shishen Yan, Lihui Bai. Phys. Rev. B., **104**, L100401 (2021). DOI: 10.1103/PhysRevB.104.L100401
[16] M.N. Iliev, D. Mazumdar, J. X. Ma, A. Gupta, F. Rigato, J. Fontcuberta. Physical Review B — Condensed Matter and Materials Physics, **83**, *1*, 014108. (2011). DOI: 10.1103/PhysRevB.83.014108
[17] A. Ahlawat, V.G. Sathe. Iournal of Raman Spectroscopy, **42**, *5*, 1087 (2011). DOI: 10.1002/jrs.2791
[18] G. Dagan, W. Shen, M. Tomkiewicz. Journal of the Electrochemical Society, **139**, *7*, 1855 (1992). DOI: 10.1149/1.2069511

[19] S. Cercelaru, A.-M. Nguyen, P. Hesto, G. Tremblay, J.-C. Perron Sever Cercelaru. J. Magn. Magn. Mater., **160**, 338 (1996). DOI: 10.1016/0304-8853(96)00220-X
[20] K. Masahiro, Y. Kazuhiro, J. Magn. Magn. Mater., **147**, *1–2*, 213 (1995). DOI: 10.1016/0304-8853(95)00022-4.
[21] M. Sousa, H. Tourinho, J.C. Rubim. Journal of Raman Spectroscopy, **31**, *3*, 185 (2000). DOI: 10.1002/(SICI)1097-4555(200003)31:3¡185::AID-JRS511¿3.0.CO;2-B
[22] O. Diaz-Morales, D. Ferrus-Suspedra, M.T. Koper. Chemical Science, **7**, *4*, 2639 (2016). DOI: 10.1039/C5SC04486C
[23] F. Tang, T. Liu, W. Jiang, L. Gan. Journal of Electroanalytical Chemistry, **871**, 114282 (2020). DOI: 10.1016/j.jelechem.2020.114282
[24] A. Ahlawat, V.G. Sathe, V.R. Reddy, A. Gupta. J. Magn. Magn. Mater., **323**, *15*, 2049 (2011). DOI: 10.1016/j.jmmm.2011.03.017
[25] B. Tsedenbal, I. Hussain, M.S. Anwar, B.H. Koo. Journal of nanoscience and nanotechnology, **18**, *9*, 6127 (2018). DOI: /10.1166/jnn.2018.15614
[26] Q. Zhang, X. Lu, L. Chen, Y. Shi, T. Xu, M. Liu. Materials Letters, **106**, 447 (2013). DOI: 10.1016/j.matlet.2013.08.029
[27] J. F. Mir, S. Rubab, M.A. Shah. Chemical Physics Letters, **741**, 137088. (2020). DOI: 10.1016/j.cplett.2020.137088
[28] R. Yang, X. Liu, H. Du, N. Sun, H. Lin, S. Li. AIP Advances, **7**, *5*, 056301 (2016). DOI: 10.1063/1.4972799
[29] A. Sikora, M. Ozimek, W. Wilczyński. Acta Physica Polonica A, **129**, *6*, 1226 (2016). DOI: 10.12693/APhysPolA.129.1226
[30] N. Cotón, J.P. Andrés, M. Jaafar, A. Begué, R. Ranchal. Journal of Applied Physics, **135**, *9*, 093905 (2024). DOI: 10.1063/5.0193531
[31] N. Cotón, J.P. Andrés, M. Jaafar, A. Begué, R. Ranchal. J. Magn. Magn. Mater., **565**, 170246 (2023). DOI: 10.1016/j.jmmm.2022.170246
[32] K. O'Grady, L.E. Fernandez, G. Vallejo-Fernandez. J. Magn. Magn. Mater., **322**, 883 (2010). DOI: 10.1016/j.jmmm.2009.12.011

Translated by E.Ilinskaya